Current Alzheimer Research, 2020, *17*, 939-947

RESEARCH ARTICLE

Directed Network Defects in Alzheimer's Disease Using Granger Causality and Graph Theory

Man Sun[1], Hua Xie[2,†] and Yan Tang[1,*,†]

[1]*School of Computer Science and Engineering, Central South University, Changsha, 410008 Hunan, People's Republic of China;* [2]*Department of Psychiatry and Behavioral Sciences, Stanford University, Stanford, CA, 94305, USA*

ARTICLE HISTORY

Received: February 19, 2020
Revised: September 19, 2020
Accepted: November 17, 2020

DOI:
10.2174/1567205017666201215140625

Abstract: ***Background:*** Few works studied the directed whole-brain interaction between different brain regions of Alzheimer's disease (AD). Here, we investigated the whole-brain effective connectivity and studied the graph metrics associated with AD.

Methods: Large-scale Granger causality analysis was conducted to explore abnormal whole-brain effective connectivity of patients with AD. Moreover, graph-theoretical metrics including small-worldness, assortativity, and hierarchy, were computed from the effective connectivity network. Statistical analysis identified the aberrant network properties of AD subjects when compared against healthy controls.

Results: Decreased small-worldness, and increased characteristic path length, disassortativity, and hierarchy were found in AD subjects.

Conclusion: This work sheds insight into the underlying neuropathological mechanism of the brain network of AD individuals such as less efficient information transmission and reduced resilience to a random or targeted attack

Keywords: Alzheimer's disease, effective connectivity, large-scale granger causality, functional connectomes, assortativity, hierarchy.

1. INTRODUCTION

Alzheimer's disease (AD) is a progressive neurodegenerative disease with a long incubation period [1]. A gradual loss of memory and a decline in cognitive ability are among the primary clinical manifestations. As the disease progresses, the patients with AD will also show language impairment, personality, and behavior changes which eventually affect their everyday lives [2, 3]. It is estimated that 5.7 million Americans have Alzheimer's dementia in 2018 [4], while in China more than seven million people live with AD [5]. However, the pathogenesis of AD is still unclear, and much research emphasis has been placed on understanding the multifactorial nature of AD.

Various neuroimaging techniques have been explored to study the pathophysiology underlying AD. Among these are positron emission tomography (PET), diffusion tensor imaging (DTI), and functional MRI (fMRI). Resting-state fMRI (rs-fMRI), which measures blood oxygenation level-dependent (BOLD) signals during rest, has been widely employed to study brain abnormalities of individuals with cognitive impairment such as AD [6], mainly relying on brain connectivity. Brain connectivity has been mainly characterized as functional connectivity (FC) and effective connectivity [7] (EC). FC measures the indirect temporal correlation between distributed brain regions [8] and a growing literature has pinpointed some key FC links with AD [9-11]. EC, albeit being more challenging to estimate, supposedly captures the causal relationship of (BOLD) signals between brain regions, providing a way to estimate the directed information flow underlying the structural pathway [7]. EC models the directed coupling of dynamic neural activity, attempting to extract causal influences of one region over another [7]. In recent years, a few studies have employed EC to study brain aberrations of AD individuals [12-16]. For example, reduced default mode network (DMN) interactions were shown in AD patients compared with healthy controls (HC) [15]. They also showed that compared with HC, the directed coupling between various brain regions was altered in AD patients. Ample research has suggested that the disease-specific change in effective connectivity throughout the brain is closely connected to neurodegenerative processes, even though such alterations may only appear in a certain part of the brain [17]. However, it is still not well understood how changes in whole-brain effective connectivity are related to AD. In addition, the works in AD, focusing on the effective connectivity of whole-brain networks are still relatively limited.

Granger causality (GC) can be used to characterize the effective connectivity in brain networks, and as a data-driven

*Address correspondence to this author at the School of Computer Science and Engineering, Central South University, Changsha, China; Tel/Fax: +86-188-7404-5262; E-mail: tangyan@csu.edu.cn
[†]*Authors share co-last authorship.*
for the Alzheimer's Disease Neuroimaging Initiative

approach, it requires no prior assumptions [18, 19]. Much of the previous research in assessing the causal relationship among brain areas has shown that GC can provide the directionality of regional activities. Granger causality mapping (GCM) is a seed-based whole-brain method that has been applied to dissect directional connectivity [20-22]. For an ROI-based whole-brain network, to avoid the ill-posed and under-determined situations when modeling whole-brain EC using GC [23, 24], large-scale Granger causality (lsGC) was used [25, 26]. After EC patterns were estimated, graph theoretical method was used to further analyze these networks to explore the pattern of information flow, which has revealed many changes of whole-brain network connections that may help identify and predict disorders in the nervous system [27]. In addition, graph theoretical approaches are receiving widespread attention in connectivity research, and many studies have found its correlations with cognition and behavior. For example, in an EC study based on GC, betweenness centrality and middleman power of some brain regions in AD were significantly correlated with behavioral measurement (such as MMSE and CDR) [28]. Graph metrics such as global efficiency and small-worldness are often studied in the brain network. Previous studies have found that compared to normal people, the brain network of AD patients presents lower small-world characteristics [29]. Graph theory is a powerful tool for analyzing the separation and integration of brain network, which will extend to the study of other psychiatric diseases [30]. However, the current topological analysis based on the directed and weighted whole-brain network has not been widely applied. In addition, more attention is needed to explore the overall performance of human brain network functions and structures, mostly the community organization, such as assortativity.

Therefore, the main themes of the paper are to investigate the causal interaction between brain regions and study the aberrations in the topology of brain networks of patients with AD. Specifically, graph theoretical method was applied to the EC networks of AD and HC to study the abnormal graph metrics. In order to study the influence of partial structure failure on the whole structure and function of the neural network, the assortative coefficient was investigated whether the topological EC network was significantly distinct in AD patients.

2. MATERIALS AND METHODS

2.1. Subjects

The rs-fMRI data of 42 subjects with AD and 42 age and gender-matched healthy subjects were obtained from the Alzheimer's disease neuroimaging initiative (ADNI) database1 (http://ADNI.loni.usc.edu). The experimental protocols carried out in this paper were approved by the ADNI Data and Publications Committee. All subjects from the database were collected according to ADNI protocol and gave an informed consent based on the Helsinki declaration. Healthy controls (HC) did not have abnormal memory loss and were provided with normal cognitive function. MMSE scores of HC were within the range of 24 to 30 and the CDR scores were zero. The enrolled AD patients were with MMSE score between 20 and 26 and CDR score to be 0.5 or 1.

2.2. Data Acquisition and Preprocessing

The functional imaging data were obtained through a 3-Tesla scanner following the ADNI protocol. The acquired fMRI data were with repetition time (TR) = 3000ms, echo time (TE) = 30ms, flip angle = 80°, in-plane resolution/voxel size = 3.313 × 3.313 × 3.313mm, slice thickness = 3.313 mm and #slice = 48. Each participant collected 140 volumes during a trial session.

We discarded the first 5 volumes before the scanner reached equilibrium, and the remaining 135 volumes underwent further analysis using SPM8 [31] (www.fil.ion.ucl.ac.uk/spm; Wellcome Trust Center for Neuroimaging, University College London, United Kingdom) and Data Processing Assistant for Resting-State fMRI advanced edition [32] (DPARSFA). The following steps were taken in preprocessing: slice time correction, head motion correction, normalization to MNI space. The rotation of all participants in any direction was within 1.5 degrees. The data were then smoothed with a 4mm-Gaussian kernel, followed by linear detrending and band-pass filtering (0.01-0.08 Hz). Subsequently, nuisance covariate regression was carried out to control the effect of nuisance signals, including six head motion parameters, white matter signal, and the cerebrospinal fluid (CSF). In order to reduce the influence of the head movement on the effective connectivity, scrubbing was performed and the linear interpolation was used to replace the images with a framewise displacement greater than 0.5 mm [33]. At last, each functional image was parcellated into 246 regions of interest (ROIs) based on the Brainnetome Atlas [34].

2.3. Effective Connectivity

To explore the causal effect between brain regions, GC analysis was employed to estimate the whole-brain information flow, which is mostly implemented in a multivariate vector autoregressive framework. Since the number of samples is smaller than the number of ROIs, multivariate vector autoregression estimation would be underdetermined and ill-posed. Therefore, the large-scale Granger causal (lsGC) method was applied [26]. The algorithm is described as follows.

(1) To reduce the redundancy of the ROI timeseries of $X = (x_1, x_2, \ldots, x_{246})$, we performed principal components analysis (PCA) and retained the first *m* components with the most variance and all time-series were projected into the low-dimensional feature space.

[1] Data used in the preparation of this article were obtained from the Alzheimer's Disease Neuroimaging Initiative (ADNI) database (adni.loni.usc.edu). The ADNI was launched in 2003 as a public-private partnership, led by Principal Investigator Michael W. Weiner, MD. The primary goal of ADNI has been to test whether serial magnetic resonance imaging (MRI), positron emission tomography (PET), other biological markers, and clinical and neuropsychological assessment can be combined to measure the progression of mild cognitive impairment (MCI) and early Alzheimer's disease (AD). For up-to-date information, see www.adni-info.org.

(2) Multivariate vector auto-regressive model with time lag q (MVAR(q)) was estimated using signals from m-dimensional feature space as follows:

$$z(t) = \sum_{j=1}^{q} A_j\, z(t-j) + e(t) \quad (1)$$

$$\hat{z}(t) = \sum_{j=1}^{q} A_j\, z(t-j) \quad (2)$$

where $z(t)$ is an ($m \times 1$) vector from the dimensionality reduced feature space; A_j is the estimated ($m \times m$) auto-regressive coefficient of j^{th} lag; $e(t)$ is an ($m \times 1$) unobservable zero mean white noise process; $\hat{z}(t)$ corresponds to the estimated time series.

(3) We removed the r[th] ROI from X, and re-estimate to the MVAR model and fitted value $\hat{z}(t)\backslash X_r$ to obtain the influence of that ROI on all other ROI time series.

(4) The error from the original model and reduced model was compared to compute the GC using the following equation after projecting back to high-dimensional signal space:

$$F_{X_s \to X_r} = \ln \frac{var(e_{X_s \backslash X_r})}{var(e_{X_s})} \quad (3)$$

where $var(e_{X_s \backslash X_r})$ is the variance of error associated with s[th] ROI without information from r[th] ROI and $var(e_{X_s})$ denotes the variance of error of s[th] ROI using the full MVAR model. If the error variance of the full model is smaller incorporating information from r[th] ROI, then X_r Granger-causes X_s.

Two hyperparameters need to be carefully selected when using lsGC method to explore the causal relationships in the brain network. One is the number of principal components to be kept, which determines how much information is retained; the other is the lag order q in the MVAR model. The number of principal components was carefully evaluated based on the cumulative curve of variance. The curve tends to be saturated as the number of principal components increases, and the range in which this saturation point determines the optimal range of the number of principal components. According to the previous studies [35, 36], a small lag order (usually on the scale of 2 to 3 seconds) was usually used when applying GC to fMRI data. The lag order (q) was set to be 2 as TR=3s in our study.

2.4. Graph Properties

The directed weighted connection network obtained from the lsGC technique was used to calculate the global properties of the network. Global properties include small-worldness, E_{global}, L_p, C_p, hierarchy [37], and multiple types of assortativity. These six parameters were described by Rubinov and Sporns [38]. For a network G with N nodes, various network attributes are characterized as below.

Clustering coefficient [39] (C_p) is the average intensity of triangles around a node and describes the degree of node aggregation in a graph, which is defined as follows:

$$C_p = \frac{1}{N} \sum_{i \in G} \frac{e_i}{k_i(k_i-1)/2} \quad (4)$$

where e_i is the number of edges connected by node i and k_i is the degree of the node i.

The characteristic path length (L_p) describes the optimal path of one node to another node and plays an important role in the transmission of the network.

We generated 1000 random networks preserving the same number of nodes, indegree and outdegree distribution as the real network to evaluate the small-world topology in the EC networks. The small-world attribute is defined as: $\sigma = \frac{\gamma}{\lambda} = \frac{C_p^{real}/C_p^{rand}}{L_p^{real}/L_p^{rand}}$, where C_p^{rand} and L_p^{rand} were obtained via averaging the 1000 corresponding random networks. A network is a small-world when $\sigma > 1$.

Global efficiency measures the capability of global information transmission of the network.

$$E_{global}(G) = \frac{1}{N(N-1)} \sum_{i \neq j \in G} \frac{1}{L_{ij}} \quad (5)$$

where L_{ij} is the shortest path length between node i and node j.

The hierarchy (β) was obtained from the ratio relationship between the nodal clustering coefficient G (local property) and nodal degrees k [37, 40]: $G \sim k^{-\beta}$. The index β was quantified by fitting a linear regression model between log(G) and log(k). A large positive value of β means that the hubs of the network have high nodal degree but low nodal clustering, indicating that the hub is well-connected while its immediate neighbors are not connected between each other, forming a "tree-like" structure. Assortativity was used to examine if vertices with similar degree/strength tend to connect to each other. In a directed and weighted network, assortativity is roughly divided into three cases: (1) in-strength assortativity, which measures the tendency of nodes with similar in-strength to be connected; (2) out-strength assortativity, which measures the tendency of nodes with similar out-strength to be connected. (3) assortativity of different directions, including the in-strength/out-strength coefficient and the out-strength/in-strength coefficient.

These graph metrics were calculated over a wide range of m (see Section Methods-Effective Connectivity) using Brain Connectivity Toolbox [38] (BCT). Prior to calculating various network measures, the EC network of each object is thresholded to a weighted sparse network. Global cost efficiency [41] defined as global efficiency minus the threshold was applied to determine an optimal threshold that depends on the dimensionality m.

2.5. Statistical Analysis

To ensure our graph analysis did not depend on the specific choice of m, we calculated the area under the curve (AUC) for each network measure. A two-sample t-test was used on the global measures of networks for the group difference between the HC and AD group. The nonparametric Mann-Whitney U test was also evaluated, given the potential difference in the variance of each group. FDR correction was used for controlling the multiple comparisons of graph measures after the tests ($p < 0.05$, FDR-corrected).

A partial correlation analysis was carried out to examine the relationships between altered network measures and clin-

Table 1. The statistic subjects and psychological assessment information. Abbreviations: MMSE: Mini-mental State Examination; CDR: Clinical Dementia Rating. Two-sample t-test was used for p-value(a), a two-tail Pearson chi-square test was used for p-value(b).

Index	HC(n=42)	AD(n=42)	*p*
Age(years)	77.7(±6.3)	75.7(±7.1)	0.177[a]
Gender(male/female)	(18/24)	(20/22)	0.157[b]
MMSE	29.0(±1.5)	21.6(±3.3)	<0.0001[a]
CDR score	0.0(±0.1)	0.9(±0.3)	<0.0001[a]

Note: a: Two-sample t-test was used for p-value, b: a two-tail Pearson chi-square test was used for p-value.

ical variables in the AD patients after controlling for age and gender.

3. RESULTS

3.1. Demographic and Psychometric Information

The rs-fMRI data of 42 AD patients and 42 age- and gender-matched healthy controls (HC) were analyzed in this study. The demographic information was summarized in Table **1**. The average disease stage estimated by the Mini-Mental State Examination (MMSE) was 21.6 ± 3.3 (mean ± std), and the average dementia severity evaluated by the Clinical Dementia Rating (CDR) score was 0.9 ± 0.3 for AD patients. The HC group had an MMSE score of 30 and a CDR score of 0.

3.2. Effective Connectivity Estimation

The large-scale Granger causal (lsGC) was applied to estimate whole-brain effective network [26], requiring two hyperparameters, lag order q and number of principal components m. The lag order q was selected to 2 based on a few studies [35, 36], and a range of principal components (m) between 20 to 37 was explored, which corresponds approximately between 75% and 90% of the explained variance [23], as shown in Fig. (**1**).

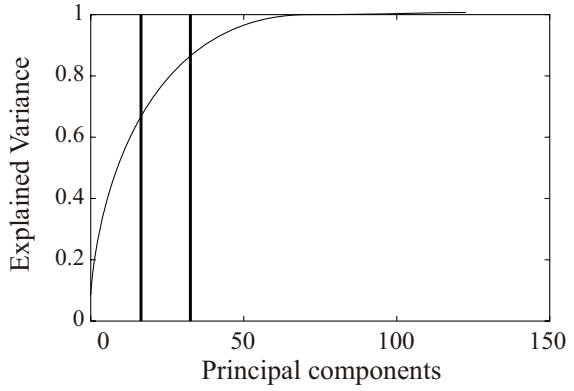

Fig. (1). This figure depicts the trend of explained variance as the number of principal components increases. In this work, we determine the number of principal components between 20 and 37, which is the solid line box, based on the trend of explained variance.

3.3. Abnormal Topological Organization of the Brain Connectome

Global cost efficiency was calculated, and the thresholds of networks were determined across different numbers of principle components. The threshold of the directed network was chosen based on the number of principle components kept [41], which varied from 0.14 to 0.17 (Fig. **2**). Graph theory approach was used to analyze the effective network. Global properties such as small-worldness (σ), global efficiency (E_{global}), characteristic path length (L_p), clustering coefficients (C_p), hierarchy (β) [37], and multiple forms of assortativity were evaluated. Generally, with an increasing number of principal components, C_p and E_{global} increased, whereas both L_p and σ decreased in both AD and HC groups (Fig. **3**). We also compared the area under the curve (AUC) of global metrics between the two groups. Two-sample *t*-test and Mann Whitney's U test showed significant group differences in four global properties. More specifically, σ (HC = 1.152±0.028, AD = 1.091±0.082, $p = 1.54\times10^{-5}$) significantly decreased in AD group, L_p (HC = 236.76±29.15, AD = 259.66±52.92, $p = 0.016$) and β (HC = 0.255±0.043, AD = 0.281±0.066, $p = 0.032$) showed significant increase in patients with AD. The assortativity (out-/in-strength correlation) (HC = -0.110±0.023, AD = -0.127±0.035, $p = 0.012$) showed negative increase in AD group (Fig. **4** and Table **2**).

No significant correlations between graph attributes and other clinical data were found.

4. DISCUSSION

We applied large-scale Granger causality (lsGC) algorithm on the rs-fMRI of patients with AD and healthy subjects to investigate the whole-brain effective connectivity (EC). Unlike the undirected functional connectivity network (FC), EC captured the directed information flow. The weighted EC networks in AD demonstrated abnormal topological properties overall, possibly revealing the mechanism underlying the aberrant cognitive function affected by AD.

The human brain has been shown to be a small-world network that maintains efficient information integration between spatially distributed brain regions. We found that such property was maintained in both normal individuals and AD patients, indicating the resilience of the human brain facing AD [42, 43]. However, the AD group showed decreased small-wordness and an abnormal topology with significantly increased characteristic path length (L_p) in comparison with control group, which coincided with the previous findings [44]. Larger L_p suggested that information transmission could be more difficult in AD patients [44]. AD patients showed an increase in the distance of information integration

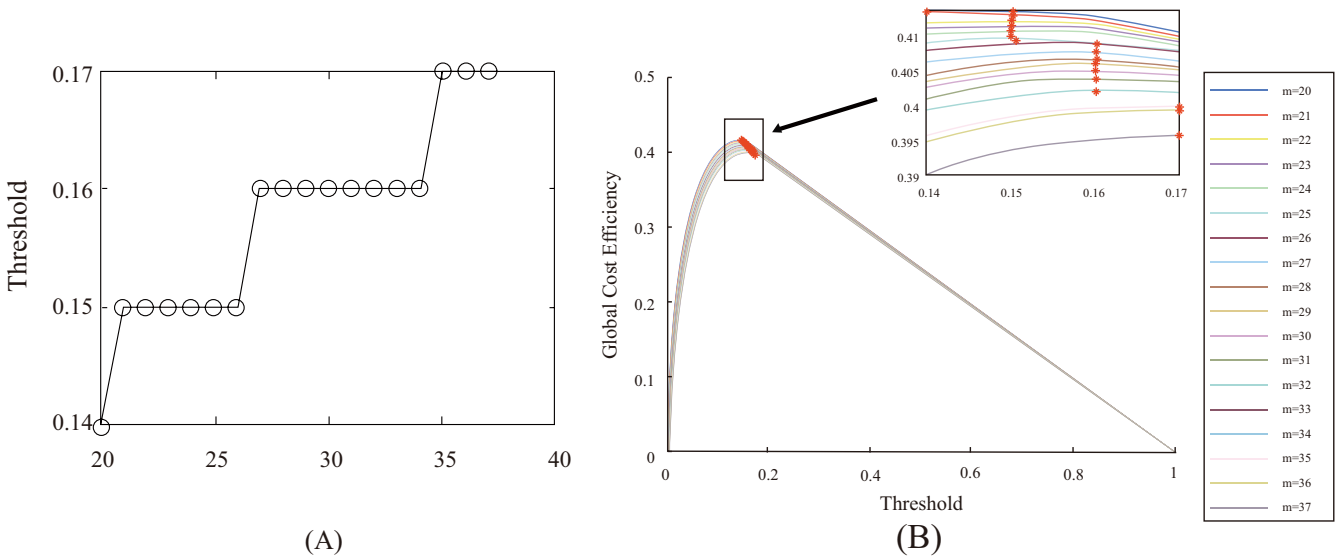

Fig. (2). The optimum values of threshold according to global cost efficiency (GCE). (**A**) shows the optimal thresholds of directed networks at different number of principle components (m). (**B**) shows the process of obtaining the optimal threshold. Each curve with color represents the change in global cost efficiency when the threshold increases in a network generated by m principal components. * is the max GCE and the corresponding thresholds. (*A higher resolution / colour version of this figure is available in the electronic copy of the article*).

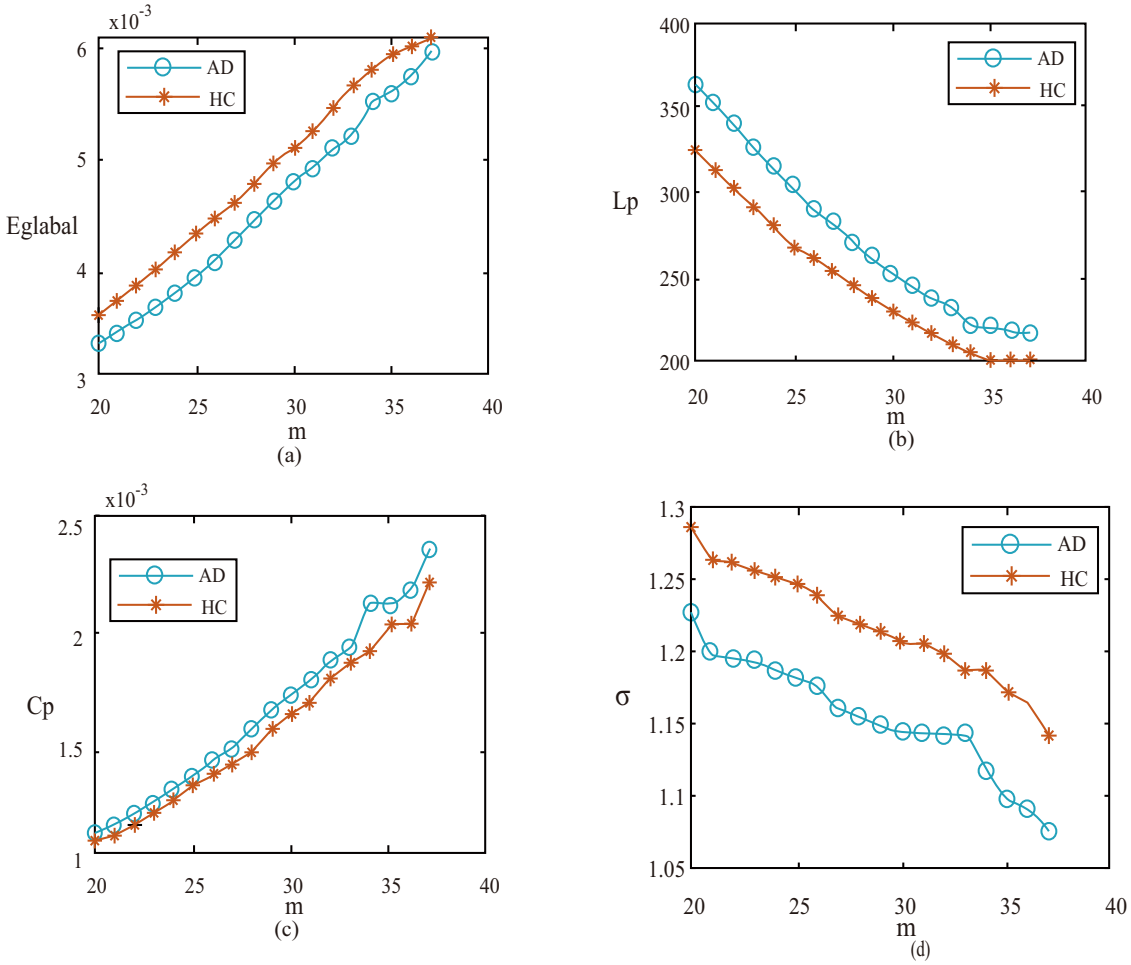

Fig. (3). This figure depicts the trend of small-world network parameters as the number of principal components increases. Every parameter was respectively averaged over HC group and AD group at every *m* value. With *m* increasing, E_{global} (**a**) and C_p (**b**) increase, while L_p (c) and σ (**d**) decrease. (*A higher resolution / colour version of this figure is available in the electronic copy of the article*).

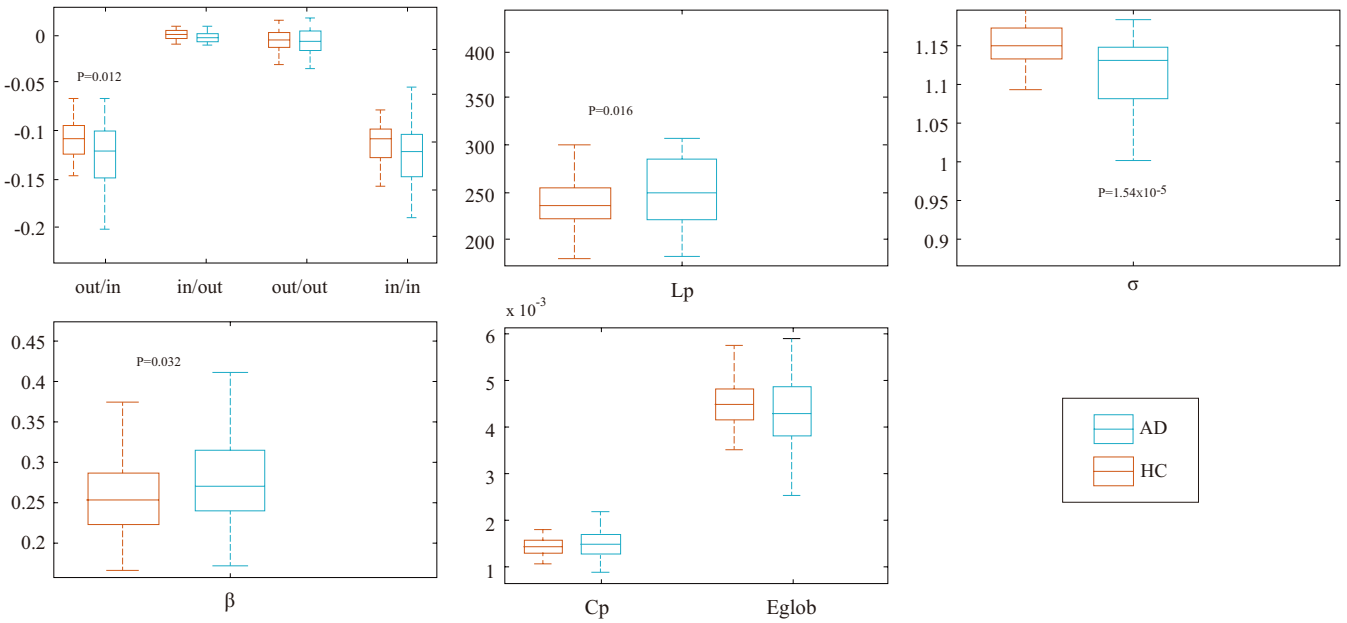

Fig. (4). Difference between HC group and AD group in global metrics. The assortativity (out-/in-strength correlation), hierarchy (β), characteristic path length (L_p) and small-worldness (σ) appear significant differences among them. (*A higher resolution / colour version of this figure is available in the electronic copy of the article*).

Table 2. Global graph measures that appear significantly different between HC and AD were calculated over different *m* values and here is the averaged AUC of these measures.

Global Measures	HC(Mean±Std)	AD(Mean±Std)	*P*
Assortativity (out-strength/in-strength)	-0.110±0.023	-0.127±0.035	0.012
Characteristic path length	236.76±29.15	259.66±52.92	0.016
Hierarchy	0.255±0.043	0.281±0.066	0.032
Small-worldness	1.152±0.028	1.091±0.082	1.54×10^{-5}

and a decrease in the ability of information transmission. This change in the AD brain network can be manifested in the patient's behaviors in many forms, such as the decline in memory or cognitive ability. In general, all cognitive activities depend on efficient information integration and transmission capabilities [45, 46]. One of the pathological changes of AD patients is that a large area of neuron death occurs in the brain [47]. In the central nervous system, the key brain regions, which participate in learning and memory storage, will be seriously damaged [48]. As a result, the information flow in many brain regions on the pathways supporting important functions may be disrupted and cause AD patients leading to decreased cognitive functions. Thus, we speculated that the impaired network of AD patients might contribute to cognitive decline, which would appear the aberrant structure with longer L_p.

As the neurodegenerative disease progresses, only the small-world properties are not enough to describe the details of its topological alterations. Therefore, we calculated the assortativity to explore the network resilience of AD patients based on directed weighted EC networks, which measures how likely it is for nodes to attach other nodes with similar nodal degree. A positive assortative coefficient indicates that nodes in a network are preferentially attached to nodes with a similar degree, signaling more efficient information processing capabilities and stronger resilience to random attacks or targeted removal of hubs [46, 49]. In a disassortative network, nodes with a high degree in general tend to be connected to nodes with a lower degree, which is more difficult for percolation relative to the corresponding assortative network [50]. However, the above-mentioned studies mostly focused on undirected functional networks. In our study, the out-/in-strength correlations were negative, and the anatomical network is disassortative in previous findings [51]. Thus, our study suggested the directed functional networks of normal subjects could not be simply characterized as assortative or disassortative, while both patterns were likely to co-exist at the same time.

In the present study, more negative assortative coefficients (out-/in-strength correlation), *i.e.* disassortativity, were found in AD patients in contrast to healthy individuals, indicating that nodes with stronger out-strength tended to connect to nodes with weaker in-strength. The phenomenon of enhanced disassortativity in AD indicates weaker resilience

of the nervous system facing neurodegeneration. This result indicates that the brain network is composed of many small modules, *i.e.* hierarchical [52, 53]. Assortativity and hierarchy are two complementary topological and structural attributes [54]. By studying the assortativity of EC networks, the hierarchical nature of EC networks can be clearly discovered. A hierarchical network is conducive to communication across different levels and requires less wiring cost, but it is also more prone to attacks (*i.e*., removal of hubs [40]). Here, the EC network of AD demonstrated a significantly increased hierarchical coefficient, which indicates excessively dispersed distribution of hubs [55]. EC network of AD patients might be limited in terms of wiring cost choices and faced a greater risk of hub removal as compared with HC. Furthermore, brain regions with high out-strength are generally more important in the EC network than brain regions with weak in-strength, and they are also higher-level brain regions from the perspective of hierarchy. Therefore, our results demonstrated that the increased disassortativity in AD could be interpreted as reduced resilience to random or targeted attacks in the EC network.

CONCLUSION

This study used lsGC to analyze the brain's effective connectome (EC) to study abnormality associated with AD. Using graph theoretic methods, we found an abnormal directed network structure in AD patients, in the form of anomalous hierarchy, and assortative coefficients. Our results shed some light into EC aberration related to the potential neuropathological mechanisms of AD patients. Given the novelty of the methodology, future investigation is warranted to validate our findings.

AUTHOR'S CONTRIBUTION

YT, MS, and HX contributed to the conception and design of the study. M.S. and Y.T. designed the experiment; M.S. and Y.T. analyzed the data; YT, MS, and HX drafted the manuscript. YT and HX participated in editing the manuscript. All authors reviewed the manuscript and approved the submitted version.

ETHICS APPROVAL AND CONSENT TO PARTICIPATE

The experimental protocols carried out in this paper were approved by the ADNI Data and Publications Committee. All subjects from the database were collected according to the ADNI protocol.

HUMAN AND ANIMAL RIGHTS

No animals were used in this study. All human procedures were performed in accordance with the guidelines of Helsinki declaration.

CONSENT FOR PUBLICATION

Informed consent was taken from patients.

AVAILABILITY OF DATA AND MATERIALS

Not applicable.

FUNDING

None.

CONFLICT OF INTEREST

The authors declare no conflict of interest, financial or otherwise.

ACKNOWLEDGEMENTS

Data used in preparation of this article were obtained from the Alzheimer's Disease Neuroimaging Initiative (ADNI) database (http://ADNI.loni.usc.edu). As such, the investigators within the ADNI contributed to the design and implementation of ADNI and/or provided data but did not participate in the analysis or writing of this report. A complete listing of ADNI investigators can be found at: http://adni.loni.usc.edu/wp-content/uploads/how_to_apply/ADNI_Acknowledgement_List.pdf. Data collection and sharing for this project was funded by the Alzheimer's Disease Neuroimaging Initiative (ADNI) (National Institutes of Health Grant U01 AG024904) and DOD ADNI (Department of Defense award number W81XWH-12-2-0012). ADNI is funded by the National Institute on Aging, the National Institute of Biomedical Imaging and Bioengineering, and through generous contributions from the following: AbbVie, Alzheimer's Association; Alzheimer's Drug Discovery Foundation; Araclon Biotech; BioClinica, Inc.; Biogen; Bristol-Myers Squibb Company; CereSpir, Inc.; Cogstate; Eisai Inc.; Elan Pharmaceuticals, Inc.; Eli Lilly and Company; EuroImmun; F. Hoffmann-La Roche Ltd and its affiliated company Genentech, Inc.; Fujirebio; GE Healthcare; IXICO Ltd.; Janssen Alzheimer Immunotherapy Research & Development, LLC.; Johnson & Johnson Pharmaceutical Research & Development LLC.; Lumosity; Lundbeck; Merck & Co., Inc.; Meso Scale Diagnostics, LLC.; NeuroRx Research; Neurotrack Technologies; Novartis Pharmaceuticals Corporation; Pfizer Inc.; Piramal Imaging; Servier; Takeda Pharmaceutical Company; and Transition Therapeutics. The Canadian Institutes of Health Research is providing funds to support ADNI clinical sites in Canada. Private sector contributions are facilitated by the Foundation for the National Institutes of Health (www.fnih.org). The grantee organization is the Northern California Institute for Research and Education, and the study is coordinated by the Alzheimer's Therapeutic Research Institute at the University of Southern California. ADNI data are disseminated by the Laboratory for Neuro Imaging at the University of Southern California. Guest or honorary authorship based solely on position (*e.g*. research supervisor, departmental head) is discouraged.

REFERENCES

[1] Blennow K, de Leon MJ, Zetterberg H. Alzheimer's disease. Lancet 2006; 368(9533): 387-403. http://dx.doi.org/10.1016/S0140-6736(06)69113-7 PMID: 16876668

[2] Costa P T. Recognition and initial assessment of Alzheimer's disease and related dementias 1996.

[3] Chatterjee A, Strauss ME, Smyth KA, Whitehouse PJ. Personality changes in Alzheimer's disease. Arch Neurol 1992; 49(5): 486-91. http://dx.doi.org/10.1001/archneur.1992.00530290070014 PMID: 1580810

[4] Association AS. Alzheimer's disease facts and figures. Alzheimers Dement 2018; 14: 367-429.

[5] Jia J, Wei C, Chen S, *et al.* The cost of Alzheimer's disease in China and re-estimation of costs worldwide. Alzheimers Dement 2018; 14(4): 483-91.
http://dx.doi.org/10.1016/j.jalz.2017.12.006 PMID: 29433981

[6] Greicius M. Resting-state functional connectivity in neuropsychiatric disorders. Curr Opin Neurol 2008; 21(4): 424-30.
http://dx.doi.org/10.1097/WCO.0b013e328306f2c5 PMID: 18607202

[7] Friston KJ. Functional and effective connectivity: a review. Brain Connect 2011; 1(1): 13-36.
http://dx.doi.org/10.1089/brain.2011.0008 PMID: 22432952

[8] Friston KJ, Frith CD, Liddle PF, Frackowiak RS. Functional connectivity: the principal-component analysis of large (PET) data sets. J Cereb Blood Flow Metab 1993; 13(1): 5-14.
http://dx.doi.org/10.1038/jcbfm.1993.4 PMID: 8417010

[9] Agosta F, Pievani M, Geroldi C, Copetti M, Frisoni GB, Filippi M. Resting state fMRI in Alzheimer's disease: beyond the default mode network. Neurobiol Aging 2012; 33(8): 1564-78.
http://dx.doi.org/10.1016/j.neurobiolaging.2011.06.007 PMID: 21813210

[10] Jalilianhasanpour R, Beheshtian E, Sherbaf G, Sahraian S, Sair HI. Functional connectivity in neurodegenerative disorders: Alzheimer's disease and frontotemporal dementia. Top Magn Reson Imaging 2019; 28(6): 317-24.
http://dx.doi.org/10.1097/RMR.0000000000000223 PMID: 31794504

[11] J L, Testa N, Jordan R, *et al.* Functional connectivity between the resting-state olfactory network and the hippocampus in Alzheimer's disease. Brain Sci 2019; 9(12): 338.

[12] Zhao S, Rangaprakash D, Venkataraman A, Liang P, Deshpande G. Investigating focal connectivity deficits in alzheimer's disease using directional brain networks derived from resting-state fMRI. Front Aging Neurosci 2017; 9: 211.
http://dx.doi.org/10.3389/fnagi.2017.00211

[13] Scherr M, Utz L, Tahmasian M, *et al.* Effective connectivity in the default mode network is distinctively disrupted in Alzheimer's disease-a simultaneous resting-state FDG-PET/fMRI study. Hum Brain Mapp 2019; doi: 10.1002/hbm.24517.

[14] Liu J, Ji J, Jia X, Zhang A. Learning brain effective connectivity network structure using ant colony optimization combining with voxel activation information. IEEE J Biomed Health Inform 2020; 24(7): 2028-2040.

[15] Zhong Y, Huang L, Cai S, *et al.* Alzheimer's Disease Neuroimaging Initiative. Altered effective connectivity patterns of the default mode network in Alzheimer's disease: an fMRI study. Neurosci Lett 2014; 578: 171-5.
http://dx.doi.org/10.1016/j.neulet.2014.06.043 PMID: 24996191

[16] Chen G, Ward BD, Chen G, Li S-J. Decreased effective connectivity from cortices to the right parahippocampal gyrus in Alzheimer's disease subjects. Brain Connect 2014; 4(9): 702-8.
http://dx.doi.org/10.1089/brain.2014.0295 PMID: 25132215

[17] Tang Y, Liu B, Yang Y, *et al.* Identifying mild-moderate Parkinson's disease using whole-brain functional connectivity. Clin Neurophysiol 2018; 129(12): 2507-16.
http://dx.doi.org/10.1016/j.clinph.2018.09.006 PMID: 30347309

[18] Friston K, Moran R, Seth AK. Analysing connectivity with Granger causality and dynamic causal modelling. Curr Opin Neurobiol 2013; 23(2): 172-8.
http://dx.doi.org/10.1016/j.conb.2012.11.010 PMID: 23265964

[19] Khazaee A, Ebrahimzadeh A, Babajani-Feremi A. Alzheimer's Disease Neuroimaging Initiative. Classification of patients with MCI and AD from healthy controls using directed graph measures of resting-state fMRI. Behav Brain Res 2017; 322(Pt B): 339-50.
http://dx.doi.org/10.1016/j.bbr.2016.06.043 PMID: 27345822

[20] Seth AK, Barrett AB, Barnett LJJN. Granger causality analysis in neuroscience and neuroimaging. J Neurosci 2015; 35(8): 3293-7.

[21] Ide JS, Chiang-Shan RL. A cerebellar thalamic cortical circuit for error-related cognitive control. Neuroimage 2011; 54: 455-64.

[22] Hu S, Job M, Jenks SK, Chao HH, *et al.* Imaging the effects of age on proactive control in healthy adults. Brain Imaging Behav 2019; 13(6): 1526-1537.

[23] Schmidt C, Pester B, Schmid-Hertel N, Witte H, Wismüller A, Leistritz L. A multivariate granger causality concept towards full brain functional connectivity. PLoS One 2016; 11(4): e0153105.
http://dx.doi.org/10.1371/journal.pone.0153105 PMID: 27064897

[24] Wismüller A, Nagarajan MB, Witte H, Pester B, Leistritz L. Pair-wise clustering of large scale Granger causality index matrices for revealing communities. Proc SPIE Int Soc Opt Eng 2014; 9038: 90381R.

[25] Nigro S, Riccelli R, Passamonti L, *et al.* Characterizing structural neural networks in de novo Parkinson disease patients using diffusion tensor imaging. Hum Brain Mapp 2016; 37(12): 4500-10.
http://dx.doi.org/10.1002/hbm.23324 PMID: 27466157

[26] DSouza AM, Abidin AZ, Leistritz L, Wismüller A. Exploring connectivity with large-scale Granger causality on resting-state functional MRI. J Neurosci Methods 2017; 287: 68-79.
http://dx.doi.org/10.1016/j.jneumeth.2017.06.007 PMID: 28629720

[27] Whitlow CT, Casanova R, Maldjian JA. Effect of resting-state functional MR imaging duration on stability of graph theory metrics of brain network connectivity. Radiology 2011; 259(2): 516-24.
http://dx.doi.org/10.1148/radiol.11101708 PMID: 21406628

[28] Zhao S, Rangaprakash D, Liang P, Deshpande GJB. Deterioration from healthy to mild cognitive impairment and Alzheimer's disease mirrored in corresponding loss of centrality in directed brain networks. Brain Inform 2019; 6: 8.

[29] Stam CJ, Jones BF, Nolte G, Breakspear M, Scheltens P. Small-world networks and functional connectivity in Alzheimer's disease. Cereb Cortex 2007; 17(1): 92-9.
http://dx.doi.org/10.1093/cercor/bhj127 PMID: 16452642

[30] Zhang Y, Zhang S, Ide JS, *et al.* Dynamic network dysfunction in cocaine dependence: Graph theoretical metrics and stop signal reaction time. Neuroimage Clin 2018; 18: 793-801.

[31] Eickhoff SB, Stephan KE, Mohlberg H, *et al.* A new SPM toolbox for combining probabilistic cytoarchitectonic maps and functional imaging data. Neuroimage 2005; 25(4): 1325-35.
http://dx.doi.org/10.1016/j.neuroimage.2004.12.034 PMID: 15850749

[32] Chao-Gan Y, Yu-Feng Z. DPARSF: a MATLAB toolbox for" pipeline" data analysis of resting-state fMRI. Front Syst Neurosci 2010; 4: 13.
PMID: 20577591

[33] Power JD, Barnes KA, Snyder AZ, Schlaggar BL, Petersen SE. Spurious but systematic correlations in functional connectivity MRI networks arise from subject motion. Neuroimage 2012; 59(3): 2142-54.
http://dx.doi.org/10.1016/j.neuroimage.2011.10.018 PMID: 22019881

[34] Fan L, Li H, Zhuo J, *et al.* The human brainnetome atlas: a new brain atlas based on connectional architecture. Cereb Cortex 2016; 26(8): 3508-26.
http://dx.doi.org/10.1093/cercor/bhw157 PMID: 27230218

[35] Marinazzo D, Liao W, Chen H, Stramaglia S. Nonlinear connectivity by Granger causality. Neuroimage 2011; 58(2): 330-8.
http://dx.doi.org/10.1016/j.neuroimage.2010.01.099 PMID: 20132895

[36] Duggento A, *et al.* Multivariate Granger causality unveils directed parietal to prefrontal cortex connectivity during task-free MRI. Sci rep-UK 2018; 8: 5571.

[37] Ravasz E, Barabási A-L. Hierarchical organization in complex networks. Phys Rev E Stat Nonlin Soft Matter Phys 2003; 67(2 Pt 2): 026112.
http://dx.doi.org/10.1103/PhysRevE.67.026112 PMID: 12636753

[38] Rubinov M, Sporns O. Complex network measures of brain connectivity: uses and interpretations. Neuroimage 2010; 52(3): 1059-69.
http://dx.doi.org/10.1016/j.neuroimage.2009.10.003 PMID: 19819337

[39] Tang Y, Xiao X, Xie H, *et al.* Altered functional brain connectomes between sporadic and familial Parkinson's patients. Front Neuroanat 2017; 11: 99.
http://dx.doi.org/10.3389/fnana.2017.00099 PMID: 29163072

[40] Bassett DS, Bullmore E, Verchinski BA, Mattay VS, Weinberger DR, Meyer-Lindenberg A. Hierarchical organization of human cortical networks in health and schizophrenia. J Neurosci 2008; 28(37): 9239-48.
http://dx.doi.org/10.1523/JNEUROSCI.1929-08.2008 PMID: 18784304

[41] Khazaee A, Ebrahimzadeh A, Babajani-Feremi A. Application of advanced machine learning methods on resting-state fMRI network for identification of mild cognitive impairment and Alzheimer's disease. Brain Imaging Behav 2016; 10(3): 799-817.
http://dx.doi.org/10.1007/s11682-015-9448-7 PMID: 26363784

[42] Sporns O, Zwi JD. The small world of the cerebral cortex. Neuroinformatics 2004; 2(2): 145-62.
http://dx.doi.org/10.1385/NI:2:2:145 PMID: 15319512

[43] Achard S, Salvador R, Whitcher B, Suckling J, Bullmore E. A resilient, low-frequency, small-world human brain functional network with

highly connected association cortical hubs. J Neurosci 2006; 26(1): 63-72.
http://dx.doi.org/10.1523/JNEUROSCI.3874-05.2006 PMID: 16399673

[44] Zhao X, Liu Y, Wang X, *et al.* Disrupted small-world brain networks in moderate Alzheimer's disease: a resting-state FMRI study. PLoS One 2012; 7(3): e33540.
http://dx.doi.org/10.1371/journal.pone.0033540 PMID: 22457774

[45] Sporns O, Chialvo DR, Kaiser M, Hilgetag CC. Organization, development and function of complex brain networks. Trends Cogn Sci 2004; 8(9): 418-25.
http://dx.doi.org/10.1016/j.tics.2004.07.008 PMID: 15350243

[46] Newman ME. The structure and function of complex networks. SIAM Rev 2003; 45: 167-256.
http://dx.doi.org/10.1137/S003614450342480

[47] Selkoe DJJPR. Alzheimer's disease: genes, proteins, and therapy. Physiol Rev 2001; 81(2): 741-66.
http://dx.doi.org/10.1152/physrev.2001.81.2.741 PMID: 11274343

[48] Lazarov O, Marr R A J E N. Neurogenesis and Alzheimer's disease: at the crossroads. Exp Neurol 2010; 223: 267-81.

[49] Davies RR, Kipps CM, Mitchell J, Kril JJ, Halliday GM, Hodges JR. Progression in frontotemporal dementia: identifying a benign behavioral variant by magnetic resonance imaging. Arch Neurol 2006; 63(11): 1627-31.
http://dx.doi.org/10.1001/archneur.63.11.1627 PMID: 17101833

[50] Newman ME. Mixing patterns in networks. Phys Rev E Stat Nonlin Soft Matter Phys 2003; 67(2 Pt 2): 026126.
http://dx.doi.org/10.1103/PhysRevE.67.026126 PMID: 12636767

[51] Park CH, Kim SY, Kim Y-H, Kim K. Comparison of the small-world topology between anatomical and functional connectivity in the human brain. Physica A 2008; 387: 5958-62.
http://dx.doi.org/10.1016/j.physa.2008.06.048

[52] Foster JG, Foster DV, Grassberger P, Paczuski M. Edge direction and the structure of networks. Proc Natl Acad Sci USA 2010; 107(24): 10815-20.
http://dx.doi.org/10.1073/pnas.0912671107 PMID: 20505119

[53] Dong G, Yang L, Li CR, *et al.* Dynamic network connectivity predicts subjective cognitive decline: the Sino-Longitudinal Cognitive impairment and dementia study. Brain Imag Behav 2020; 14(6): 2692-707.
http://dx.doi.org/10.1007/s11682-019-00220-6 PMID: 32361946

[54] de Haan W, Pijnenburg YA, Strijers RL, *et al.* Functional neural network analysis in frontotemporal dementia and Alzheimer's disease using EEG and graph theory. BMC Neurosci 2009; 10: 101.
http://dx.doi.org/10.1186/1471-2202-10-101 PMID: 19698093

[55] Dong G, *et al.* Dynamic network connectivity predicts subjective cognitive decline: the Sino-Longitudinal Cognitive impairment and dementia study. Brain Imag Behav 2020; 14(6): 2692-07.